RSC Advances

PAPER

View Article Online
View Journal | View Issue

Cite this: *RSC Adv.*, 2025, **15**, 14307

Kinetic study on the hydrogenation of dimethyl succinate to γ-butyrolactone†

Chenghao Zhao, ‡[a] Chengzhe Du,‡[b] Huixia Ma,*[a] Rui Jiang,[a] Huanling Zhang[a] and Feng Zhou[a]

Received 20th February 2025
Accepted 10th April 2025

DOI: 10.1039/d5ra01226k

rsc.li/rsc-advances

The hydrogenation of dimethyl succinate (DMS) to γ-butyrolactone (GBL) is crucial in producing high-value chemicals for pharmaceuticals, agrochemicals, and battery electrolytes. This study utilized a self-developed copper-based catalyst and a micro-fixed bed reactor to systematically investigate the effects of temperature, pressure, and the hydrogen-to-ester ratio on reaction performance. An intrinsic kinetic model was developed based on experimental data, with reaction rate constants and activation energies determined through standard regression techniques. The model correlated well with observed data, providing insights into reaction kinetics. Validation against experimental data indicated fair agreement across various conditions. Sensitivity analysis confirmed the model's robustness, making it useful for process optimization. This kinetic analysis offers insights to enhance the efficiency and cost-effectiveness of industrial GBL production, aiming to improve overall process yield and efficiency.

1 Introduction

γ-Butyrolactone (GBL), also known as 1,4-butyrolactone, is an important chemical intermediate with wide-ranging applications in pharmaceuticals,[1,2] solvents,[3,4] battery production,[5,6] and petrochemicals.[7,8] Approximately 70% of GBL's production capacity is utilized for the synthesis of *N*-methylpyrrolidone (NMP),[9] which serves as a key solvent in lithium battery manufacturing. With the rapid development of the new energy vehicle industry in China, the demand for NMP is expected to rise steadily in the future.

Currently, the majority of GBL production is derived from the dehydrogenation of 1,4-butanediol (BDO), which is typically produced *via* the acetylene-based route.[10] This method, using calcium carbide as a raw material, falls into the category of "high pollution, high energy consumption, and high carbon emissions", indicating significant limitations for its future applications. In contrast, the phthalic anhydride esterification and hydrogenation route demonstrates lower emissions, allowing for the co-production of GBL and tetrahydrofuran (THF) alongside BDO.[11] Additionally, China's phthalic anhydride production capacity has been continuously increasing, resulting in lower raw material costs, thereby presenting a promising application outlook for this route.

Dimethyl succinate (DMS), a product of the hydrogenation of the esterification product dimethyl maleate (DMM), can be further hydrogenated to selectively produce GBL. By modifying the catalyst composition and process conditions, it is possible to achieve either a high yield or a selective production of GBL. The employment of copper-based catalysts for the gas-phase hydrogenation of DMS offers mild operating conditions, a straightforward process, and favorable selectivity and yield.[12–14] Many studies have shown that Cu(II)-based catalysts have the following advantages: low cost, environmentally friendly, high selectivity for the cleavage of C–O bonds, low activity for the cleavage of C–C bonds, and excellent activation capability for hydrogen molecules. These characteristics make Cu(II)-based catalysts widely applicable in catalytic reactions, especially in the fields of green chemistry and sustainable development.[15–21]

Numerous studies have been conducted on the reactors,[22,23] catalysts,[24,25] processes,[26,27] and stability[28] associated with the hydrogenation of DMM or DMS, as well as related reaction kinetics.[29,30] For example, Chaudhari[31] investigated the kinetics of the gas–solid phase reaction of diethyl maleate using a cuprous chromate catalyst, deriving rate constants and activation energies for different reactions within this network. Similarly, Zhang Qi[32] examined the gas–solid phase reaction kinetics of diethyl succinate with a copper-based catalyst, obtaining relevant kinetic parameters. However, both studies utilized a power-law kinetic model and operated at pressures exceeding 2 MPa, during which multiple products, including GBL, BDO, THF, and *n*-butanol, were present.

In contrast, there has been limited intrinsic kinetic research on the selective or multiple production of GBL from DMS under

[a]*SINOPEC Dalian Research Institute of Petroleum and Petrochemicals Co., Ltd, Dalian 116100, China. E-mail: zhaochenghao.fshy@sinopec.com*

[b]*State Key Laboratory of Multiphase Complex Systems, Institute of Process Engineering, Chinese Academy of Sciences, Beijing 100190, China. E-mail: czdu@ipe.ac.cn*

† Electronic supplementary information (ESI) available. See DOI: https://doi.org/10.1039/d5ra01226k

‡ Co-first authors.

low-pressure conditions. Therefore, this study employs a copper-based catalyst to conduct gas–solid phase catalytic reaction kinetics experiments while eliminating internal and external diffusion limitations. The aim is to elucidate the reaction mechanism for the hydrogenation of DMS to predominantly produce GBL and to derive the parameters for the corresponding hyperbolic intrinsic kinetic model, providing a reference for the reactor design for GBL production *via* DMS hydrogenation.

2 Materials and methods

2.1 Materials

Dimethyl succinate (DMS, 99%) was obtained from J&K Scientific Technology Co., Ltd; hydrogen gas (99.999%) was sourced from Dalian Special Gases Co., Ltd; methanol, γ-butyrolactone, 1,4-butanediol, and tetrahydrofuran, all of chromatographic purity, were purchased from Shanghai Macklin Biochemical Technology Co., Ltd.

2.2 Catalyst

The metal composition of the catalyst consists of Cu, Zn, and Al, referred to as CuZnAl. The specific preparation steps can be found in the ESI.† Additionally, we conducted a systematic characterization of the catalyst, including the crystalline phase structure (Fig. S1†), textural properties (Fig. S2 and Table S1†), the form of copper present (Fig. S3†), reduction properties (Fig. S4†), and morphology (Fig. S5†). Detailed characterization results and analysis are available in the ESI.†

2.3 Experimental setup and procedure

The schematic diagram of the micro fixed-bed hydrogenation apparatus used in the experiment is shown in Fig. 1.

A fixed-bed reactor with an inner diameter of approximately 8 mm and a length of 120 mm was utilized in this study. The catalyst, after crushing and screening, was uniformly mixed with inert quartz sand and packed in the middle section of the reactor, maintaining a packing height of 50 mm, with inert quartz sand above and below. Hydrogen was introduced into the reactor from the upper end, controlled by a mass flow meter. The fixed bed was then heated to 240 °C according to a programmed schedule and maintained at this temperature for 6 hours to ensure complete activation of the catalyst. Dimethyl succinate (DMS) was delivered into the top of the reactor through a plunger pump along with hydrogen. After passing through a preheater, the DMS came into contact with the catalyst in the fixed bed for the reaction. The reaction pressure was maintained using a backpressure valve. The products were discharged to a constant pressure product tank after passing through a secondary condenser, while the off-gases were directed to the utility venting line.

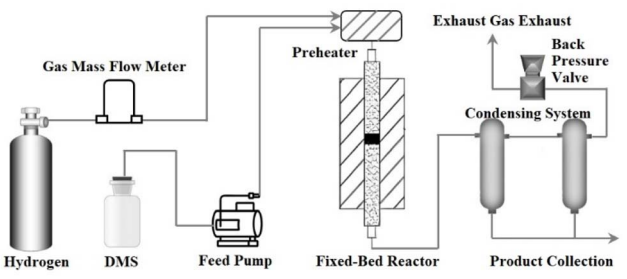

Fig. 1 Schematic diagram of the micro fixed-bed hydrogenation apparatus.

2.4 Product analysis method

The analysis of reactants and products was conducted using an Agilent 8860 gas chromatograph equipped with a capillary column (50 m × 320 μm × 1.2 μm), featuring a stationary phase of 5% diphenyl-95% dimethyl polysiloxane. Quantitative analysis was performed using the area normalization method. The vaporization chamber temperature was set to 250 °C, and the detector temperature was maintained at 300 °C. The temperature programming for the column was as follows: initial temperature at 100 °C with a hold time of 5 minutes; heating rate of 10 °C min^{-1} to 160 °C with a hold time of 1 minute; followed by a heating rate of 10 °C min^{-1} to 280 °C with a hold time of 3 minutes.

The calculation formulas for various evaluation indicators of catalyst activity are as follows:

$$\text{Conversion rate of DMS}(X) = \frac{n_{\text{DMS0}} - n_{\text{DMS}}}{n_{\text{DMS0}}} \times 100\%$$

$$\text{Selectivity of product}(i)(S) = \frac{n_{\text{i}}}{n_{\text{DMS0}} - n_{\text{DMS}}} \times 100\%$$

In the expression, n_{DMS0} represents the number of moles of DMS in the feed; n_{DMS} denotes the number of moles of DMS in the product; and n_{i} indicates the number of moles of DMS converted into product i.

3 Kinetic model development and parameter fitting

3.1 Preliminary experiments

During the hydrogenation of DMS, reaction conditions such as pressure, temperature, and hydrogen-to-ester ratio significantly influence conversion rates and product distribution. To better define the range of experimental conditions for the hydrogenation of DMS to synthesize GBL, preliminary experiments were conducted to investigate the effects of these process parameters on the reaction.

3.1.1 Temperature. Under conditions of LHSV = 0.2 h^{-1} and a pressure of 1 MPa, the influence of temperature on product distribution was examined, as shown in Fig. 2. As the reaction temperature increased, the conversion rate of DMS also gradually improved, particularly between 200 °C and 210 °C, where the most significant enhancement was observed. This behavior can be attributed to the fact that the vaporization temperature of DMS at atmospheric pressure is approximately 200 °C. Under a reaction pressure of 1 MPa, even in the presence of hydrogen, some DMS remains unvaporized below 210 °C. Therefore, to ensure that the reaction consistently occurs in a gas–solid phase catalytic system, subsequent kinetic experiments were conducted at temperatures above 210 °C.

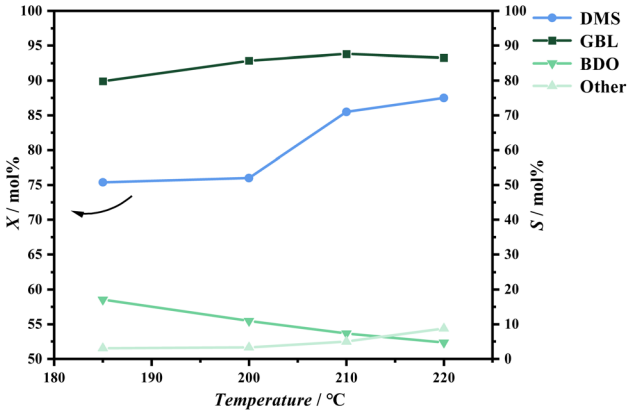

Fig. 2 Effect of temperature on reaction activity.

Regarding product distribution, as the temperature increased, the selectivity for GBL gradually rose while the selectivity for BDO decreased. This trend can be explained by the endothermic nature of the DMS hydrogenation to GBL and the exothermic reaction of GBL hydrogenation to BDO. The elevation in temperature favors the forward reaction of DMS hydrogenation, which aligns with previously published thermodynamic studies.[33]

3.1.2 Pressure. Under conditions of LHSV = 0.2 h^{-1} and a temperature of 210 °C, the effect of pressure on product distribution was examined, as illustrated in Fig. 3. It is evident that the selectivities for both GBL and BDO are quite sensitive to pressure. This sensitivity arises from the fact that BDO is a product of the further hydrogenation of GBL. Higher pressure conditions favor the additional hydrogenation of GBL, thereby reducing its selectivity. Consequently, for subsequent kinetic modeling aimed at optimizing either exclusive or multiple production of GBL, the reaction pressure was controlled to remain below 1.6 MPa.

3.1.3 Hydrogen to ester ratio. Under conditions of LHSV = 0.2 h^{-1}, a temperature of 210 °C, and a pressure of 1.6 MPa, the effect of the molar ratio of hydrogen to dimethyl succinate in the feed on product distribution was investigated. It was observed that increasing the hydrogen to ester ratio under these conditions had negligible impact on product selectivity;

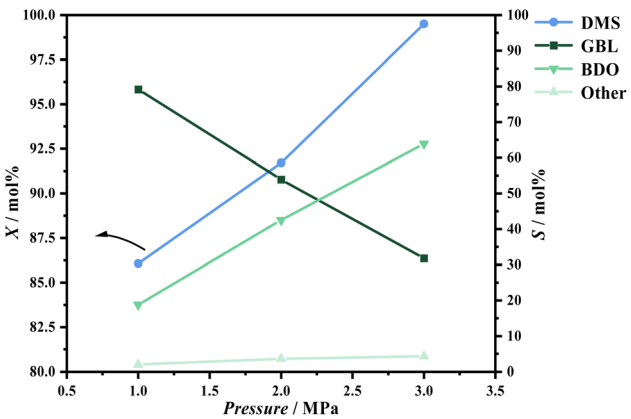

Fig. 3 Effect of pressure on reaction activity.

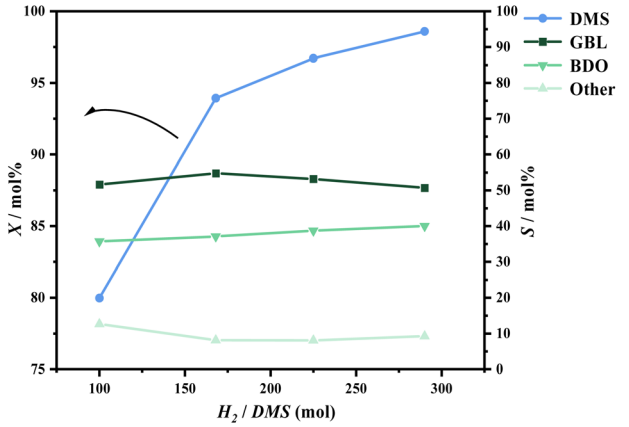

Fig. 4 Effect of hydrogen to ester ratio on reaction activity.

however, the conversion rate of DMS significantly increased at higher hydrogen to ester ratios. For the purposes of the kinetic experiments, it is undesirable for the reactants to achieve complete conversion, even in a continuous stirred-tank reactor. Therefore, in subsequent investigations, the hydrogen to ester ratio was maintained below 100 (Fig. 4).

3.2 Assumptions for kinetic pathways and model development

3.2.1 DMS hydrogenation network. Considering the investigation of process conditions for the selective production of GBL or the co-production of by-products during DMS hydrogenation in preliminary experiments, it was observed that under relatively mild hydrogenation conditions, the concentrations of THF, *n*-butanol, and other by-products were minimal. Therefore, in the subsequent model development and data fitting analysis, only the reaction pathways of DMS hydrogenation to GBL and GBL hydrogenation to BDO were considered. A schematic representation of the hydrogenation network is shown in Fig. 5.

Qin[34] noted that most hydrogenation reactions involve the dissociative adsorption of hydrogen on active sites. Li[35] also concluded in their kinetic analysis of dimethyl oxalate hydrogenation that hydrogen needs to adsorb dissociatively in order to react with the ester moiety. Consequently, we assume the existence of intermediate product B ($C_5H_8O_3$) in the pathway from DMS to GBL, and intermediate product E ($C_4H_8O_2$) in the pathway from GBL to BDO. This assumption aims to make the subsequent mechanistic derivation more aligned with reality and to avoid the occurrence of unreasonable reaction orders in elementary reactions.

3.2.2 Intrinsic kinetic model. Based on the aforementioned reaction pathways, the main and side reactions are defined as follows:

$$\text{Main reaction}: \ \mathrm{DMS(A)} + 2\mathrm{H_2} \xrightarrow{k_1} \mathrm{GBL(D)} + \mathrm{MeOH(C)} \quad (1)$$

$$\text{Side reaction}: \ \mathrm{GBL(D)} + 2\mathrm{H_2} \underset{k_3}{\overset{k_2}{\rightleftharpoons}} \mathrm{BDO(F)} \quad (2)$$

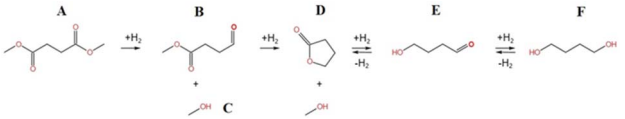

Fig. 5 Schematic representation of the DMS hydrogenation reaction network.((A) DMS; (B) $C_5H_8O_3$; (C) methanol; (D) GBL; (E) $C_4H_8O_2$; (F) BDO).

Using the Langmuir–Hinshelwood (LH) model to describe the adsorption and desorption of reactants, products, and hydrogen, the reaction mechanism is subsequently proposed based on the Hougen–Watson (HW) model, in which hydrogen undergoes dissociative adsorption.[36] The main reaction mechanism for the hydrogenation of DMS to GBL is outlined as follows:

$$H_2 + \sigma \overset{K_H}{\rightleftharpoons} 2H\sigma \quad (3)$$

$$A + \sigma \overset{K_A}{\rightleftharpoons} A\sigma \quad (4)$$

$$A\sigma + 2H\sigma \overset{k_1}{\rightarrow} B\sigma + C\sigma + \sigma \quad (5)$$

$$B\sigma + 2H\sigma \overset{k_\infty}{\rightarrow} D\sigma + C\sigma + \sigma \quad (6)$$

$$C\sigma \overset{K_C}{\rightleftharpoons} C + \sigma \quad (7)$$

$$D\sigma \overset{K_D}{\rightleftharpoons} D + \sigma \quad (8)$$

Since we did not detect products B and E in our preliminary experiments, we can assume that within the experimental conditions, the rate of the reaction of B to form GBL and MeOH is effectively infinite, indicating that B does not accumulate. Based on this assumption, the elementary reactions (5) and (6) can be considered irreversible processes.[31]

Similarly, the intermediate product E can be approached with the same approximation. The side reaction mechanism for the further hydrogenation of GBL to BDO is outlined as follows:

$$D\sigma + 2H\sigma \underset{k_\infty}{\overset{k_2}{\rightleftharpoons}} E\sigma + 2\sigma \quad (9)$$

$$E\sigma + 2H\sigma \underset{k_3}{\overset{k_\infty}{\rightleftharpoons}} F\sigma + 2\sigma \quad (10)$$

$$F\sigma \overset{K_F}{\rightleftharpoons} F + \sigma \quad (11)$$

Assuming that the surface reaction of DMS hydrogenation in step (5) is the rate-controlling step of the main reaction, the intrinsic rate equation can be expressed as follows:

$$r_1 = \frac{k_1 K_A P_A K_H P_H}{\left(1 + K_A P_A + \sqrt{K_H P_H} + K_D P_D + K_C P_C + K_F P_F\right)^3} \quad (12)$$

Similarly, the rate equation for the reversible hydrogenation of GBL in the side reaction can be expressed as:

$$r_2 = \frac{k_2 K_D P_D K_H P_H - k_3 K_F P_F}{\left(1 + K_A P_A + \sqrt{K_H P_H} + K_D P_D + K_C P_C + K_F P_F\right)^3} \quad (13)$$

In the equations, k_1, k_2 and k_3 represent the reaction rate constants, while K_A, K_H, K_C, K_D and K_F are the corresponding adsorption equilibrium constants. P_A, P_H, P_C, P_D and P_F denote the partial pressures of DMS, hydrogen, methanol, GBL, and BDO, respectively.

$$r_1 = \frac{dX_A}{d(W/F_{DMS0})}$$

$$r_2 = (1 - S_D)\frac{dX_A}{d(W/F_{DMS0})} - X_A\frac{dS_D}{d(W/F_{DMS0})}$$

Assuming that the molar flow rate of dimethyl succinate (DMS) in the feed is F_{DMS0}, and that the molar ratio of hydrogen to dimethyl succinate in the feed is a, the molar flow rates of each component F_i and the total molar flow rate F_T can be determined based on the conversion of dimethyl succinate (X_A) and the selectivity of γ-butyrolactone (S_D). The expressions for these molar flow rates are as follows:

$$F_{DMS} = F_{DMS0}\cdot(1 - X_A)$$

$$F_{H_2} = F_{DMS0}\cdot[a - 2\cdot X_A - 2\cdot(1 - S_D)\cdot X_A]$$

$$F_{GBL} = F_{DMS0}\cdot X_A\cdot S_D$$

$$F_{BDO} = F_{DMS0}\cdot X_A\cdot(1 - S_D)$$

$$F_{MeOH} = 2\cdot F_{DMS0}\cdot X_A$$

$$F_T = F_{DMS} + F_{H_2} + F_{GBL} + F_{BDO} + F_{MeOH} = F_{DMS0}\cdot(a + 2\cdot X_A\cdot S_D - 2\cdot X_A + 1)$$

The partial pressures of each component can be calculated using the formula $\left(P_i = P\frac{F_i}{F_T}\right)$. For example:

$$P_{GBL} = P\cdot\frac{F_{GBL}}{F_T} = P\cdot(X_A\cdot S_D)/(a + 2\cdot X_A\cdot S_D - 2\cdot X_A + 1)$$

Similarly, the partial pressures of the other components can be determined. When considering factors such as temperature, pressure, and the hydrogen-to-ester ratio, the parameter estimation (fitting) problem for the resulting system of nonlinear ordinary differential equations can be expressed as follows:

$$\begin{cases} \dfrac{dX_A}{d\left(\dfrac{W}{F_{DMS0}}\right)} = f_1(X_A,\ S_D, (k_1,\ k_2,\ k_3,\ K_A, \ldots, K_F),\ a,\ P,\ T) \\ \dfrac{dS_D}{d\left(\dfrac{W}{F_{DMS0}}\right)} = f_2(X_A,\ S_D, (k_1,\ k_2,\ k_3,\ K_A, \ldots, K_F),\ a,\ P,\ T) \end{cases}$$

wherein, $\frac{dX_A}{d\left(\frac{W}{F_{DMS0}}\right)} = r_1$; $\frac{dS_D}{d\left(\frac{W}{F_{DMS0}}\right)} = [(1 - S_D)\cdot r_1 - r_2]/X_A$.

3.2.3 Elimination of internal diffusion experiments. Prior to conducting kinetic experiments, it is essential to perform experiments to eliminate internal diffusion. Catalysts with particle sizes of 10–20 mesh, 20–28 mesh, and 28–35 mesh were selected to conduct hydrogenation experiments of DMS under identical conditions. It was determined that internal diffusion was eliminated when the DMS conversion rate and product distribution remained unchanged with varying catalyst particle sizes. Tables 1, S2 and S3† present the results of the internal diffusion elimination experiments, which indicate that internal diffusion can be considered eliminated when the catalyst mesh size is greater than 20 mesh (0.84 mm). Given the narrow inner diameter of the microreactor and to minimize pressure drop associated with smaller catalyst particles, catalysts in the 20–28 mesh range were selected for subsequent kinetic studies.

3.2.4 External diffusion elimination experiments. For fixed-bed reactors, the influence of external diffusion can be eliminated or minimized by increasing the feed line velocity.[37,38] To this end, 1 g, 1.5 g, and 2 g of the catalyst (20–28 mesh) were mixed with inert quartz sand of the same mesh size. The packed bed height was set at 50 mm, and after reduction activation, the reaction was conducted at a temperature of 220 °C, a pressure of 1 MPa, and a hydrogen-to-ester ratio of 65. The trend of DMS conversion rates at the same space velocity but different linear velocities is illustrated in Fig. 6. It can be observed that under the selected experimental conditions, the DMS conversion rate does not change with variations in the linear velocity of the feed gas. Therefore, it can be confirmed that when the linear velocity exceeds 18.97×10^{-2} m s^{-1}, the influence of external diffusion can be considered negligible. Consequently, all subsequent kinetic experiments were conducted at linear velocities above this threshold to ensure that the experimental data were not affected by diffusion limitations.

3.2.5 Determination of intrinsic kinetics. Intrinsic reaction kinetics data were measured under conditions where both internal and external diffusion effects were eliminated. A catalyst with a mesh size of 20 to 28 was selected and mixed with quartz sand of the same mesh size before being packed into the central section of the reactor, with a packing height of 50 mm. This configuration ensures that the reactor diameter is more than ten times the catalyst particle diameter and that the bed height is more than fifty times the catalyst particle diameter, allowing for a plug flow model to be applicable to the gas flow within the reactor.

Table 1 Effect of catalyst particle size on the hydrogenation reaction of DMS[a]

Number of catalyst mesh	W/F_{DMS0}/(g h mol^{-1})	X_A/mol%	S_D/mol%
10–20	42.98	78.67	94.50
20–28	42.35	81.32	95.16
28–35	42.53	81.75	94.97

[a] Reaction conditions: temperature = 220 °C; pressure = 1 MPa; H_2/DMS (mol) = 65.

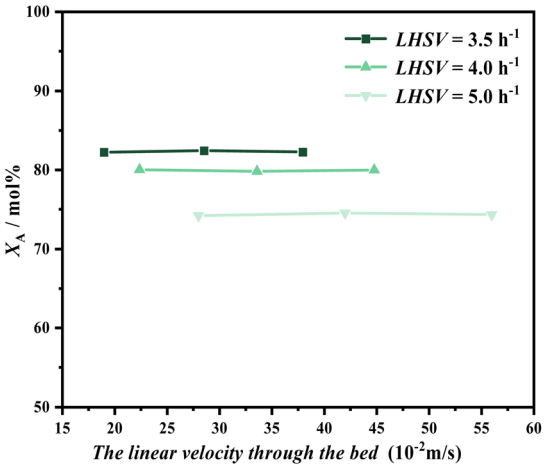

Fig. 6 Effect of external diffusion on the DMS conversion rate.

Based on the conclusions from preliminary experiments, we selected reaction temperatures ranging from 210 to 230 °C, pressures from 0.5 to 1.5 MPa, and a hydrogen-to-ester ratio of 40 to 65 for the kinetic experiments. The experimental data were fitted to the derived kinetic model, with the results shown in the figure below, where X_A' and S_D' represent the fitted curves.

At a reaction temperature of 210 °C, the conversion rate of DMS and the distribution of hydrogenation products followed the trends observed in the preliminary experiments. As pressure and the hydrogen-to-ester ratio increased, X_A significantly increased, while S_D appeared to increase with decreasing pressure. The hydrogen-to-ester ratio seemed to have a minimal impact on the distribution of GBL in the product (Fig. 7).

At a reaction temperature of 220 °C and a pressure of 1.1 MPa, the results are similar to those observed at 210 °C; an increase in the hydrogen-to-ester ratio promotes the conversion of DMS, while it has minimal impact on the selectivity for GBL. However, when the hydrogen-to-ester ratio is held constant, a notable effect on conversion rate is observed at pressures below 1.1 MPa. At pressures above 1.1 MPa, the increase in conversion rate is not significant. The selectivity for GBL remains sensitive to changes in pressure, showing a marked increase as pressure decreases.

At a reaction temperature of 230 °C, the conversion rate of DMS and the distribution of products follow a trend similar to that observed at 210 °C. Tables S4–S6† present the experimental conditions and raw data results for chemical reaction kinetics.

The residual sum of squares between the model-calculated values of DMS conversion rate and GBL selectivity and the experimental values was used as the objective function. The fitting was performed using the SLSQP (Sequential Least Squares Programming) method from the Scipy library, applying the continuous least squares approach to estimate the reaction kinetic parameters.[39] The reaction rate constants and

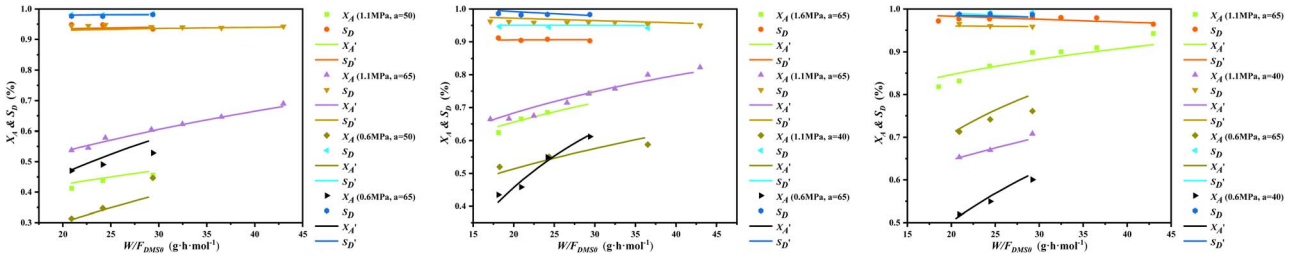

Fig. 7 Experimental and fitted values of DMS hydrogenation conversion and selectivity at 210 °C (left), 220 °C (middle) and 230 °C (right).

Table 2 Kinetic model parameters

T/K	483.15	493.15	503.15
k_1/(mol g^{-1} h^{-1})	0.6059	0.7965	1.0358
k_2/(mol g^{-1} h^{-1})	0.0504	0.1341	0.3432
k_3/(mol g^{-1} h^{-1})	19.3750	40.3571	81.6451
$K_H \times 10^{-2}$/MPa$^{-0.5}$	2.4072	2.1368	1.9059
$K_A \times 10^{-2}$/MPa^{-1}	32.8646	23.6396	17.2282
$K_C \times 10^{-2}$/MPa^{-1}	17.3760	15.2191	13.4004
$K_D \times 10^{-2}$/MPa^{-1}	6.9455	3.7633	2.0893
$K_F \times 10^{-2}$/MPa^{-1}	0.6972	0.6553	0.6174

adsorption equilibrium constants obtained from the fitting at different temperatures are presented in Table 2.

As shown in Table 2, the reaction rate constants k_1, k_2 and k_3 increase with rising temperature, while the adsorption equilibrium constants K_H, K_A, K_C, K_D and K_F decrease as the temperature increases. Among these, the rate constant for the dehydrogenation of BDO to GBL is the highest, whereas the rate constant for the hydrogenation of GBL to BDO is the lowest. The adsorption rate constants for DMS and methanol are relatively high, while the adsorption rate constants for GBL and BDO are notably low. This suggests that the adsorption of GBL and BDO on the catalyst is more challenging, allowing them to diffuse out of the solid catalyst's pores more easily, which makes them less likely to be converted to THF or *n*-butanol through deep hydrogenation, thus resulting in higher selectivity for GBL.

Based on the Arrhenius equation $k = A\exp[-E_a/(RT)]$, a linear regression of $\ln k$ against T was performed to obtain the pre-exponential factor A and the apparent activation energy E_a, with the results presented in Table 3.

As indicated in Table 3, the activation energy for the hydrogenation of DMS to GBL is significantly lower than that for the further hydrogenation of GBL to BDO. This finding is consistent with the experimental results obtained in this study, suggesting that the hydrogenation of DMS occurs more readily. Under relatively high-temperature and low-pressure conditions, the selectivity for GBL remains above 90%. Additionally, the activation energy for the dehydrogenation of BDO to GBL is also lower than that for the hydrogenation of GBL to BDO. Therefore, it can be concluded that with a moderate increase in temperature, the reverse reaction of BDO dehydrogenation proceeds more easily, favoring the increased or selective production of GBL.

Table 3 Pre-exponential factors and activation energies for hydrogenation and dehydrogenation reactions

k_i	A/(mol g^{-1} h^{-1})	E_a/(kJ mol^{-1})
k_1	4.379×10^5	54.19
k_2	4.46×10^{19}	193.74
k_3	1.02×10^{17}	145.36

3.2.6 Validation of the reaction kinetic model. The obtained kinetic parameter values were substituted into eqn (12) and (13). The fourth-order Runge–Kutta method was employed to solve the differential equations, yielding the conversion rate of DMS and the selectivity of GBL. The comparison between the calculated values of DMS conversion and GBL selectivity with the experimental values is presented in Fig. 8 and 9. It is evident that the fitting error for the conversion rate of DMS is relatively small, whereas the fitting error for GBL selectivity is somewhat larger.

A significance test was conducted on the obtained model to assess its overall capability to represent the experimental data. Given that the kinetic model is nonlinear, statistical methods suitable for nonlinear models were employed for the validation,[40] with the results presented in Table 4. It is generally accepted that a coefficient of determination R^2 greater than 0.9 and a statistical F-value greater than $10F_{0.01}$ indicate a highly suitable model. The results in Table 4 demonstrate that the model is highly suitable and can effectively describe the kinetic characteristics of the DMS hydrogenation reaction.

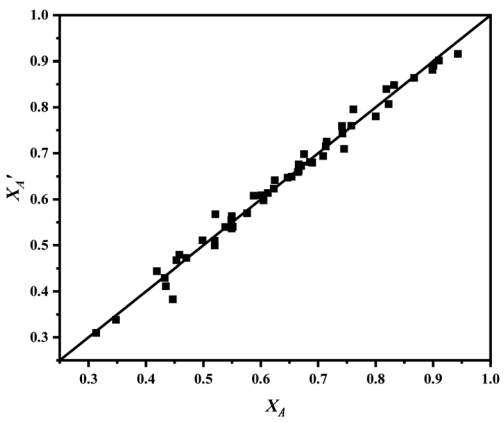

Fig. 8 Comparison of experimental and calculated values for DMS conversion rate.

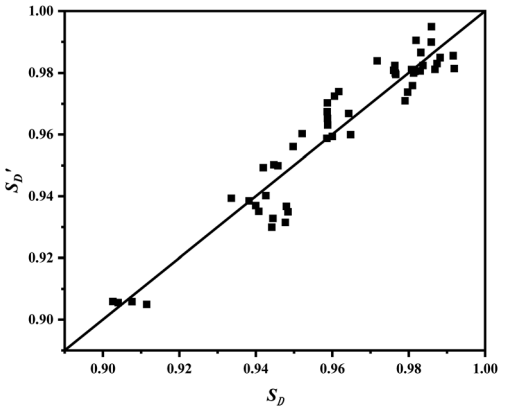

Fig. 9 Comparison of experimental and calculated values for GBL selectivity.

Table 4 Results of statistical validation

Index	R^2	F	$F_{0.01(N,N-M-1)}$
X_A	0.9854	862.14	2.97
S_D	0.9141	546.37	2.97

A significance test was conducted on the obtained model to assess its overall capability to represent the experimental data. Given that the kinetic model is nonlinear, statistical methods suitable for nonlinear models were employed for the validation,[40] with the results presented in Table 4. It is generally accepted that a coefficient of determination R^2 greater than 0.9 and a statistical F-value greater than $10F_{0.01}$ indicate a highly suitable model. The results in Table 4 demonstrate that the model is highly suitable and can effectively describe the kinetic characteristics of the DMS hydrogenation reaction.

4 Conclusions

In conclusion, this study provides a detailed kinetic analysis of the hydrogenation of dimethyl succinate (DMS) to γ-butyrolactone (GBL) using a copper-based catalyst. The intrinsic kinetic model developed offers significant insights into the reaction mechanisms and provides essential parameters for process optimization. The study identified the critical factors influencing DMS conversion and GBL selectivity, including temperature, pressure, and the hydrogen-to-ester ratio, which were systematically investigated to develop a reliable kinetic model. The developed model showed good agreement with experimental data, indicating its robustness and applicability for process design.

The findings suggest optimal reaction conditions for maximizing GBL yield, providing practical guidelines for industrial-scale production. Future research should focus on broader catalyst ranges, multi-phase reaction environments, long-term stability, and advanced analytical methods to further validate and extend the kinetic model. Overall, this research contributes to the field of catalytic hydrogenation by offering a detailed kinetic understanding and practical insights for the efficient production of γ-butyrolactone (GBL). The derived kinetic parameters and model can serve as valuable references for designing and optimizing industrial reactors, ultimately enhancing the efficiency and cost-effectiveness of GBL production.

Data availability

The data supporting this article have been included as part of the ESI.†

Author contributions

Chenghao Zhao: investigation, data curation, writing – original draft. Chengzhe Du: investigation, formal analysis. Huixia Ma: projecet administration, visualization. Rui Jiang and Huanling Zhang: methodology, validation. Feng Zhou: writing – review & editing, supervision, resources, conceptualization.

Conflicts of interest

The authors have declared no conflict of interest.

Acknowledgements

This work was supported by the National Natural Science Foundation of China (22078311) and China Petroleum & Chemical Corporation Enterprise Support Project (223051). The catalyst evaluation apparatus (dual channel catalyst fast evaluation apparatus EMC-1) was provided by the Oushisheng Company.

Notes and references

1 F. Vandescheur and L. H. Staal, *Appl. Catal., A*, 1994, **108**, 63–83.
2 R. A. Kitson, A. Millemaggi and R. K. Taylor, *Angew. Chem., Int. Ed.*, 2009, **48**, 9426–9451.
3 J. Li, Y. Zhou, J. Tian, L. Peng and W. Chu, *J. Mater. Chem. A*, 2020, **8**, 10386–10394.
4 B. Liang, B. Li, R. Jin and T. Cheng, *J. Shanghai Norm. Univ., Nat. Sci.*, 2021, **50**, 629–635.
5 X. Cai, S. Zhang, Y. Fang, Q. Liu and W. Tan, *Chem. Reagents*, 2019, **41**, 767–772.
6 L. Yang and G. Song, *Fine Spec. Chem.*, 2020, **28**, 11–14.
7 B. Huang, T. Wang, C. Lei, W. Chen, G. Zeng and F. Maran, *J. Catal.*, 2016, **339**, 14–20.
8 G. H. M. Rao and F. A. Khan, *Synth. Commun.*, 2018, **48**, 1–5.
9 X. Cui, *Technol. Econ. Petrochem.*, 2023, **39**, 57–62.
10 B. Zhang, F. Bai, P. Shi and J. Gao, *Refin. Chem. Ind.*, 2024, **35**, 6–9.
11 J. Huang, C. Chen, C. Wei and C. Zhang, *Chem. World*, 2023, **64**, 409–414.
12 T. Li, T. Zhang, J. Huang, X. Zhang and H. Wang, *Appl. Chem. Ind.*, 2023, **52**, 2192–2197+2201.

13 T. Turek, D. L. Trimm, D. S. Black and N. W. Cant, *Appl. Catal., A*, 1994, **116**, 137–150.
14 M. Mokhtar, C. Ohlinger, J. H. Schlander and T. Turek, *Chem. Eng. Technol.*, 2001, **24**, 423–426.
15 A. Dandekar and M. A. Vannice, *J. Catal.*, 1998, **178**, 621–639.
16 S. S. Acharyya, S. Ghosh and R. Bal, *Chem. Commun.*, 2014, **50**, 13311–13314.
17 B. Sarkar, C. Pendem, L. N. S. Konathala, R. Tiwari, T. Sasaki and R. Bal, *Chem. Commun.*, 2014, **50**, 9707–9710.
18 M. B. Gawande, A. Goswami, F. O. X. Felpin, T. Asefa, X. Huang, R. Silva, X. Zou, R. Zboril and R. S. Varma, *Chem. Rev.*, 2016, **116**, 3722–3811.
19 S. Jin, H. Byun and C. H. Lee, *J. Catal.*, 2021, **400**, 195–211.
20 G. Totarella, R. Beerthuis, N. Masoud, C. Louis, L. Delannoy and P. E. D. Jongh, *J. Phys. Chem. C*, 2021, **125**, 366–375.
21 F. A. Rollier, V. Muravev, A. Parastaev, R. C. J. van de Poll, J. M. J. J. Heinrichs, B. Ligt, J. F. M. Simons, M. C. Figueiredo and E. J. M. Hensen, *ACS Catal.*, 2024, **14**, 13246–13259.
22 T. Dong, B. Wang, P. Zhou, Y. Wang, J. Guo and X. Han, *Chem. Eng. Equip.*, 2024, **5**, 33–35+49.
23 M. Bradac, J. Dudas, M. Kotora and J. Markos, *Chem. Zvesti*, 2014, **68**, 1667–1677.
24 A. L. Figueredo, C. S. Costa, M. L. Gothe, L. M. Rossi, R. C. Bazito, P. Vidinha and C. G. Pereira, *Catal. Lett.*, 2021, **151**, 1821–1833.
25 H. Wang, G. Gao and Z. Du, *Spec. Petrochem.*, 2017, **34**, 36–39.
26 Y. Li, *Chem. Ind.*, 2022, **40**, 43–52.
27 X.-Q. Han, Q.-F. Zhang, F. Feng, C.-S. Lu, L. Ma and X.-N. Li, *Chin. Chem. Lett.*, 2015, **26**, 1150–1154.
28 W. Lei, A. Nuermaimaiti, M. Yubo, Q. Shaojun, G. Zhixian and E. Wumanjiang, *React. Kinet. Mech. Catal.*, 2014, **112**, 117–129.
29 G. Ding, Y. Zhu, H. Zheng, W. Zhang and Y. Li, *Catal. Commun.*, 2010, **11**, 1120–1124.
30 M. A. Kohler, M. S. Wainwright, D. L. Trimm and N. W. W. Cant, *Ind. Eng. Chem. Res.*, 1987, **26**, 652–656.
31 R. V. Chaudhari, R. Jaganathan, S. H. Vaidya, S. T. Chaudhari and C. V. Rode, *Chem. Eng. Sci.*, 1999, **54**, 3643–3651.
32 Q. Zhang and Z. Wu, *Chin. J. Catal.*, 1991, **12**, 346–352.
33 W. Liu, L. Wu and Z. Zhao, *Shanghai Chem. Ind.*, 2007, **32**, 12–16.
34 R. Qin, L. Zhou, P. Liu, Y. Gong and N. Zheng, *Nat. Catal.*, 2020, **3**, 1–7.
35 S. Li, Y. Wang, J. Zhang, S. Wang and X. Ma, *Ind. Eng. Chem. Res.*, 2015, **54**, 1243–1250.
36 I. B. Ju, W. Jeon, M. J. Park, Y. W. Suh, D. J. Suh and C. H. Lee, *Appl. Catal., A*, 2010, **387**, 100–106.
37 C. Perego and S. Peratello, *Catal. Today*, 1999, **52**, 133–145.
38 S. A. Shankha, G. Shilpi, T. Ritesh, P. Chandrashekar and S. Takehiko, *ACS Catal.*, 2015, **5**, 2850–2858.
39 J. Xue, M. Cui, J. Tang, X. Chen and X. Qiao, *Chem. React. Eng. Technol.*, 2010, **26**, 296–302.
40 T. Su, X. Zhou, Z. Qin and H. Ji, *Chemphyschem*, 2017, **18**, 299–309.